Brazilian Journal of Geophysics 42 (2024), 1, 1–15
Brazilian Geophysical Society
ISSN 2764-8044
DOI: 10.22564/brjg.v41i2.2304

ACCESSING HORIZON PICKING UNCERTAINTY USING COMPLEX SEISMIC TRACE ATTRIBUTES

Fernando Jardim [1,2*], Alexandre Maul [1] and Wagner Moreira Lupinacci [2]

[1]Petrobras, Rio de Janeiro, RJ, Brazil
[2]Universidade Federal Fluminense - UFF, Departamento de Geologia e Geofísica, Niterói, RJ, Brazil

*Corresponding author email: fernando.jardim@petrobras.com.br

ABSTRACT. Many uncertainty sources are linked to the reservoir modeling processes, significantly affecting all phases of the exploration, development, and production phases of an oil & gas field. Structural uncertainty due to velocity models are commonly considered by taking a range of equiprobable domain conversion velocity models and evaluating the related impact on GRV distributions. In contrast, the seismic interpretation inaccuracy is commonly neglected because of the difficulty in quantifying it. This means that seismic mapping is frequently treated as having no variation or having the intrinsic imprecisions arbitrarily assigned. In this work, we propose an objective approach to evaluate the horizon picking uncertainties, which was based on the extraction of complex seismic trace attributes considering a previously mapped reference reflector. In real seismic data, phase distortions may arise from a vast bunch of reasons, such as dispersion, attenuation, bandwidth limitations. Thus, the instantaneous phase attribute can be an indicator of uncertainties associated with seismic reflector interpretation.

Keywords: seismic phase distortions; complex trace; seismic attribute analysis; structural uncertainty.

INTRODUCTION

Many uncertainty sources are linked to the reservoir modeling processes, which can have significant impact on all phases of the exploration, development, and production phases of an oil & gas field. Macdonald et al. (2009) split them into three main groups: (i) Gross rock volume (GRV) uncertainty; (ii) volume of hydrocarbons in place (HCIP) uncertainty; (iii) Reserve uncertainty. GRV uncertainties are generally the most significant within reservoir modeling processes. According to Charles et al. (2001), the GRV variations are mainly associated with the velocity models used for time-depth conversion (seismic time migration) and with seismic interpretation (horizon picking). This concept using depth seismic data (seismic depth migration) instead of time seismic data (seismic time migration) is discussed in recent works (Maul et al., 2021a, 2021b; Camargo et al., 2023). Although depth positioning models have the greatest impact on GRV uncertainties (Samson et al., 1996), the uncertainties related to horizon picking are also significant and mandatory to be evaluated.

Recent works (Meyer Viol and Hoetz, 2015; Paes et al., 2019; Maul et al., 2021a, 2021b) take into account structural uncertainty due to velocity models by generating a range of equiprobable conversion models, which are used to evaluate the impact of this uncertainty on GRV distributions in a relatively direct way. In contrast, the impact of seismic interpretation uncertainty is commonly neglected, due to the difficulty in quantifying it, especially when opting for a qualitative approach with a conceptual and subjective basis, as described by Leahy and Skorstad (2013). In this type of approach, the interpreter is the responsible for classifying areas of greater or lesser uncertainty during the seismic interpretation stage, associating them with a higher-level geological concept. It means, for instance, that distinct structural framework scenarios must respect the deformational style of the area as well as the regional geological configuration. Despite the advantages of identifying uncertainties with this type of approach, it is a very laborious and time-consuming process, especially when dealing with large areas of study. Furthermore, because of the subjective bias, this type of study does not allow comparisons among different reservoirs and its success depends on the experience of the interpreters.

Another approach is to carry out the uncertainty analysis after the seismic interpretation step in a quantitative way. It is based on the fact that seismic waves are affected by several phenomena during propagation, such as geometric spreading, energy partitioning at interfaces, tuning effects, dispersion and attenuation (Simm and Bacon, 2014). According to these authors, these effects may be reduced but not eliminated during seismic processing. In this case, as proposed by Pinto et al. (2017), seismic attributes are used to identify the presence of these distortions in the data, representing the uncertainty by a vertical seismic resolution map weighted by the quality of the seismic image.

When picking a reflector, interpreters generally make three assumptions regarding the seismic response of a given interface: (i) known, (ii) stationary, and (iii) zero-phased. However, in real seismic data, the zero-phase assumption is commonly violated due to a variety of reasons, and the identification of regions where this violation occurs is the main core of this work.

We propose an approach to evaluate seismic interpretation uncertainties based on the extraction of complex seismic trace attributes in a previously mapped reference reflector. We applied the proposed methodology in synthetic seismic data and used the delivered information to assess the relevance of this uncertainty in relation to the GRV variation looking at various built scenarios. Later, after applying the methodology in real data, the obtained results showed that the horizon picking uncertainty introduced variations of the order of 5% in the GRV.

FOUNDATION

Seismic method inherent distortions

As seismic waves propagate through the subsurface, various effects attenuate the amplitudes and distort the waveform. These effects are related to (Yilmaz, 2001; Simm and Bacon, 2014):

(1) geometric spreading;

(2) dissipation;

(3) scattering.

Geometric spreading, also referred as wavefront divergence, occurs when the wavefront moves away from the source since the energy initially released is spread over an increasing area. It is a natural effect of attenuating the amplitude, proportional to $1/r$ (where r is the radius of the wavefront) (Yilmaz, 2001).

Dissipation, also referred as absorption, anelastic attenuation or intrinsic attenuation, is the exponential decay of amplitude with distance (Müller et al., 2010) and mainly results from the loss/transformation of propagation energy into heat, due to the internal friction between fluids that fill the pores, and the matrix, induced by the propagation of the seismic wave. High-frequency wave components are more attenuated than low-frequency components, resulting in pulse broadening and consequent lower resolution. However, in the frequency range of surface seismic data, from 5 to 100 Hz, the dissipation is relatively constant and generally small (Liner, 2012).

Scattering, also referred as dispersion, elastic attenuation, or apparent attenuation, is the variation of propagation velocity with frequency (Müller et al., 2010; Liner, 2012). It occurs due to the redistribution of energy caused by medium heterogeneities (Bouchaala et al., 2019), more specifically related to the presence of elastic interfaces (layering), when the wave field experiences phenomena such as reflection, transmission, multiples and mode conversion. These phenomena continuously deform the signal due to the progressive reduction of the higher frequencies and the variation in the travel velocity of each harmonic (Rosa, 2018). Frequency dependence is complex, but high frequencies lose energy much faster than low frequencies (Liner, 2012).

Dissipation and scattering are interrelated effects and are simply called attenuation (Wang, 2008). Experimentally, it has been observed that attenuation has an approximately linear dependence with frequency (Barton, 2007, as cited in Nunes et al., 2011); therefore, the constant Q attenuation model is commonly used (Kolsky, 1956, Kjartansson, 1979; as cited in Nunes et al., 2011). This model is very suitable as the attenuation property of the medium can be described using a single parameter, assumed constant: the quality factor Q, defined by the ratio between the transmitted energy (E) and the lost energy (ΔE) during a period equivalent to one cycle (T) of a frequency component of the wave (Yilmaz, 2001; Nunes et al., 2011; Rosa, 2018; Wu et al., 2022):

$$Q = \frac{2\pi E}{\Delta E}. \tag{1}$$

which can be rewritten as a function of period T and time t, as follows (Wu et al., 2022):

$$Q = \frac{2\pi E}{T\frac{dE}{dt}}. \qquad \frac{dE}{E} = \frac{2\pi}{TQ}dt\,. \tag{2}$$

$$E = E_0 e^{-\frac{2\pi t}{TQ}}.$$
$$E = E_0 e^{-\frac{2\pi f}{Qv}x}. \quad (3)$$
$$E = E_0 e^{-\alpha x}.$$

Where E_0 is the energy initially transmitted, f is the frequency, and v is the wave propagation velocity; x is the propagation distance and the term α is defined as the attenuation coefficient, which can be used as an index of the energy attenuation. As the value of α decreases, the energy loss also decreases:

$$\alpha = \frac{2\pi f}{Qv}. \quad (4)$$

Equation 4 shows that attenuation is linearly dependent to frequency. The dissipation effect attenuates more high-frequency wave components than those low-frequency ones. On the other hand, the dispersion effect causes high-frequency wave components to travel faster than the low-frequency ones, and the wavelet phase varies along the travel path (Wang, 2008), thus modifying the pulse shape.

Convolutional model

The propagation of seismic energy on Earth is a complex phenomenon, involving attenuation, geometric spreading, multiples and wave conversion effects, besides noise. Ideally, most of these effects are removed from the data during seismic processing (Simm and Bacon, 2014), allowing seismic amplitude to be related to geology (rock property contrasts).

In Figure 1 a geological sketch is represented on the left by a rock layer with acoustic impedance (velocities and densities) smaller than the one of the host rock layer. This is converted to the time domain using one theoretical velocity model and can be represented only by the acoustic impedance contrasts, resulting in a reflectivity series, R. After convolving this reflectivity series to a zero-phase wavelet, considering a normal incidence of a plane wave, and ignoring the noise effects of wave propagation, we have the synthetic seismic trace, S. The modeled seismic trace is the initial link between geology and geophysics during seismic interpretation.

Figure 1 illustrates the convolutional model, which is implicit in the minds of interpreters. From this model, included within the synthetic seismogram and the seismic-well tie processes, the interpreter obtains knowledge of the seismic response of the geological interfaces of interest.

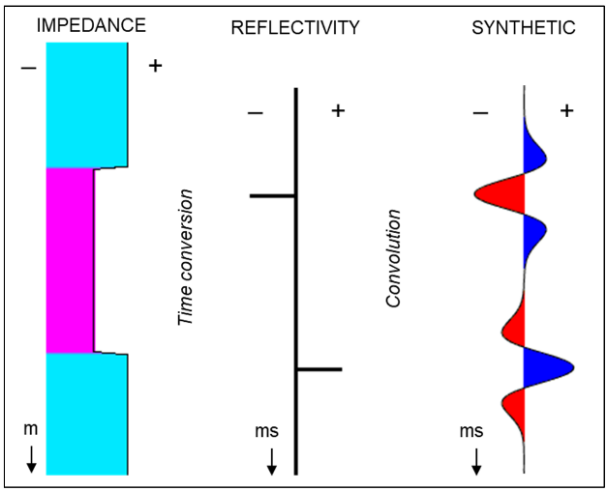

Figure 1: The convolutional model (SEG convention). In the impedance track, the light blue represents an increasing of impedance and the purple represents a decreasing of impedance. In the synthetic track, the colors dark blue and red represent positive and negative polarities, respectively.

A seismic trace can be expressed as a complex function $z(t)$, which combines the signal itself, $x(t)$, and its imaginary component (or quadrature), $iy(t)$, calculated from the Hilbert transform (Roden and Sepúlveda, 1999; Hardage, 2010):

$$z(t) = x(t) + iy(t). \quad (5)$$

The complex trace is represented by a vector that continuously changes its size and rotation (Souza et al., 2017). This concept is illustrated in Figure 2 where the real seismic trace $x(t)$, its imaginary component $y(t)$ and the complex seismic trace $z(t)$ are shown in a three-dimensional space (x, y, t).

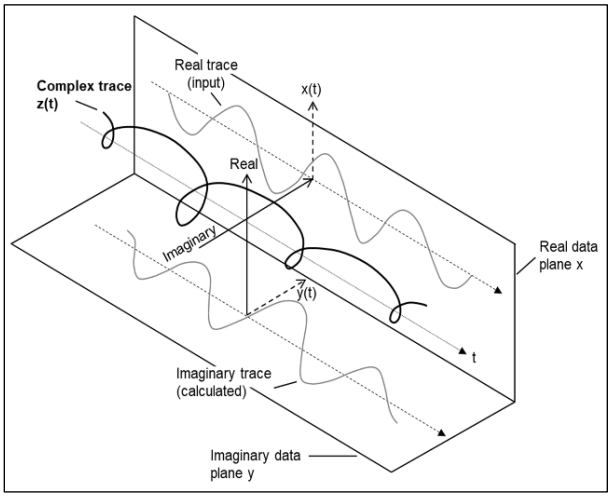

Figure 2: Representation of a complex seismic trace: real part $x(t)$ and imaginary part $y(t)$ that are added in a vector sense, resulting in the helical spiral $z(t)$. After Hardage (2010).

From the complex representation of the seismic trace, it is possible to calculate, for any coordinate of the time axis t, the magnitude and the angle of the vector perpendicular to the time axis until it intercepts the complex trace $z(t)$, as shown in Figure 1. The magnitude of this vector defines the amplitude (or envelope) of the complex trace $a(t)$:

$$a(t) = \sqrt{x^2(t) + y^2(t)}, \tag{6}$$

and the angle that vector makes with the real plane defines the phase $\Phi(t)$ of the trace:

$$\Phi(t) = tan^{-1}\left(\frac{y(t)}{x(t)}\right). \tag{7}$$

The rate of change of the instantaneous phase is the instantaneous frequency, which can be expressed in radians per second as angular instantaneous frequency $\omega(t)$ or in hertz as ordinary instantaneous frequency $f(t)$, through the relationship $\omega = 2\pi f$ (Hardage, 2010; Liner, 2012):

$$\omega(t) = \frac{d}{dt}\Phi(t). \tag{8}$$

$$f(t) = \frac{d\Phi(t)}{2\pi\, dt}. \tag{9}$$

These parameters are called **instantaneous attributes** as they can be calculated at any instant of time (t).

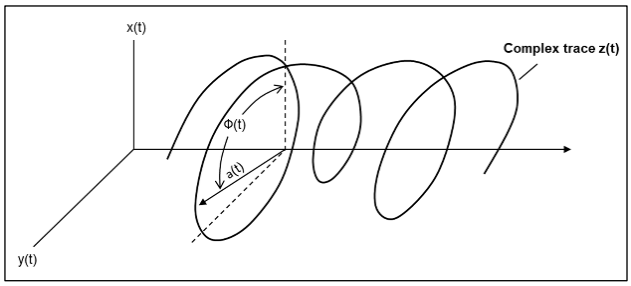

Figure 3: Instantaneous seismic attributes: the instantaneous amplitude $a(t)$ is the magnitude of the vector perpendicular to the time axis that intersects the complex trace $z(t)$; the instantaneous phase $\Phi(t)$ is the angle that this vector makes with the real plane. The instantaneous frequency $\omega(t)$ is determined by the rate of change of the instantaneous phase. After Hardage (2010).

Phase, frequency and displacement relationship

The phase of the seismic trace is expressed in terms of angles, which can be measured in degrees or radians. As it is cyclic (360 degrees), a positive phase of 150º is equivalent to a negative phase of 210º, so it is normally expressed from -180º to +180º. The phase shift has two effects on the seismic signals: the change of the relative amplitudes of the wavelet peaks and troughs and the time shift of the main peak, proportionally to the phase shift. A negative phase shift delays the main peak; a positive phase rotation advances the time of the main peak (Simm and White, 2002). These effects are illustrated in Figure 4.

The most critical parameter for seismic reflector picking is the time of the wavelet main lobe relative to time zero. Note in Figure 4 that the reflector representing the top of a layer (dotted line) matches with the mappable reflector only in the case of zero-phase wavelet. If the data are not zero-phased, there will be a difference between the time of the real reflector and the time of the mapped reflector.

Considering a band-pass analytic signal, if the instantaneous frequency of the signal is f, the time delay of the main peak corresponding to a phase shift Φ is given by (Boashash, 2016):

$$t = -\frac{\Phi}{2\pi \cdot f}. \tag{10}$$

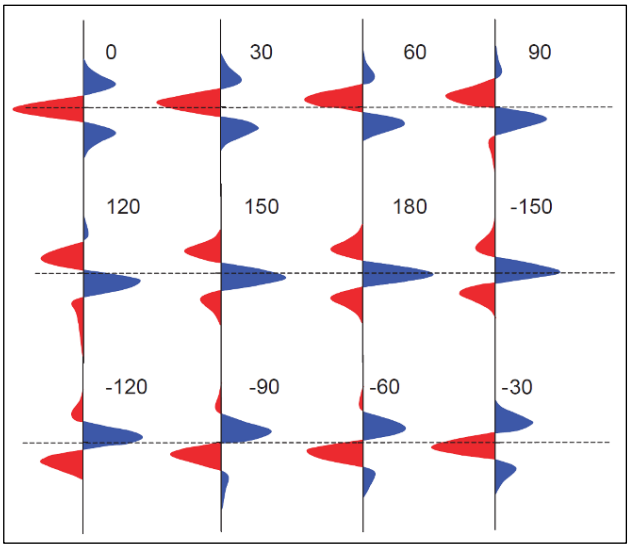

Figure 4: Phase change of a zero-phase wavelet. Simm and White (2002).

In Figure 5 the graphs illustrate the relationships among frequency, phase, time and space. Equation 10 was used to obtain the graph in Figure 5a, illustrating the relationship between frequency and time shift for various phase changes. It is observed that the lower relative frequencies will have higher time shifts for the same phase shift. The relationship between time shift and depth shift for different layer velocities is illustrated in Figure 5b. Layers with higher velocities will have greater depth shifts for the same time shift.

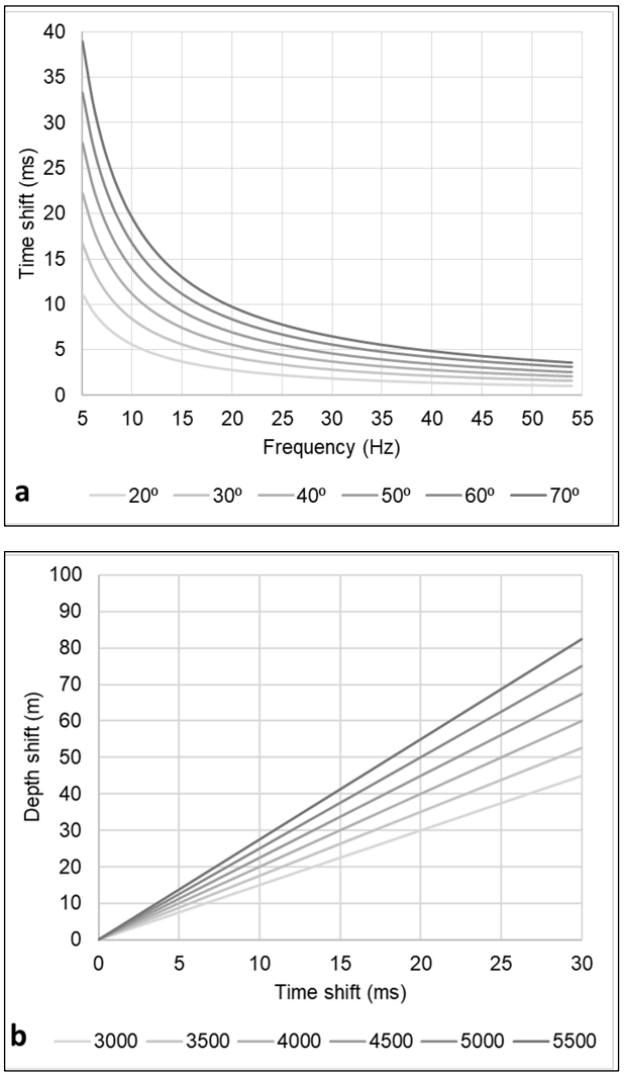

Figure 5: a) frequency and time shift relations for various phase changes; b) time shift and depth shift relations for various phase changes.

Phase as an attribute associated with uncertainty

When interpreting a seismic reflector, interpreters generally make three assumptions: that the seismic response of a given interface is (i) known, (ii) stationary, and (iii) zero-phase. Knowledge comes from the generation of a synthetic seismogram and the seismic-well tie processes. Synthetic seismograms relate physical changes in geology to a modeled seismic response; stationarity comes from the assumption that the seismic response identified in the wells represents the same geological interface even when the interpretation moves away from the wells; and zero-phase considers that the seismic processing was effective in converting the seismic pulse from mixed phase to zero-phase.

But in real seismic data, despite best efforts to control the phase of a wavelet during the acquisition and processing steps, the zero-phase assumption is commonly violated (van der Baan, 2008). Phase distortions arise due to a variety of reasons, such as dispersion, attenuation and bandwidth limitations (Levy and Oldenburg, 1987).

Phase is an attribute normally used as an indicator of continuity because it is independent of amplitude. It has greater sensitivity to faults, fractures, dislocations and other structural and stratigraphic seismic features. Although some of the geology-induced phase changes can be easily identified, such as spatial discontinuities associated with faults and incised channels, phase changes of condensed sections and erosive unconformities can be quite subtle (Matos et al., 2010).

The presence of phase distortions may not be directly related to geology, being the result, for example, of seismic processing residues (Roden and Sepúlveda, 1999). Furthermore, interpolation and/or smoothing processes of the picked horizons can eventually shift the horizon in time, not measuring correctly the expected instantaneous phase of the seismic data. We understand that all these factors place the instantaneous phase attribute as an adequate indicator of uncertainties associated with seismic reflector interpretation.

METHODOLOGY

The proposed methodology is illustrated in Figure 6 and it consists on identifying and mapping a reference interface, whose seismic response is known, preferably with high amplitude and good lateral continuity, according to Roden and Sepúlveda (1999). The instantaneous phase and frequency attributes are calculated and extracted on the mapped reference surface. Then, equation 10 is applied, generating a map of time shifts corresponding to the phase shifts, with positive and negative values. The module of this map is taken as the uncertainty indicator in the time domain, being referred as "two-way time uncertainty map". Finally, this map is converted from the time domain to the depth domain by multiplying by the compressional velocity map.

RESULTS AND DISCUSSION

Application to synthetic data

In the evaporitic section of the Campos and Santos Basins there are regional basal layers of anhydrite.

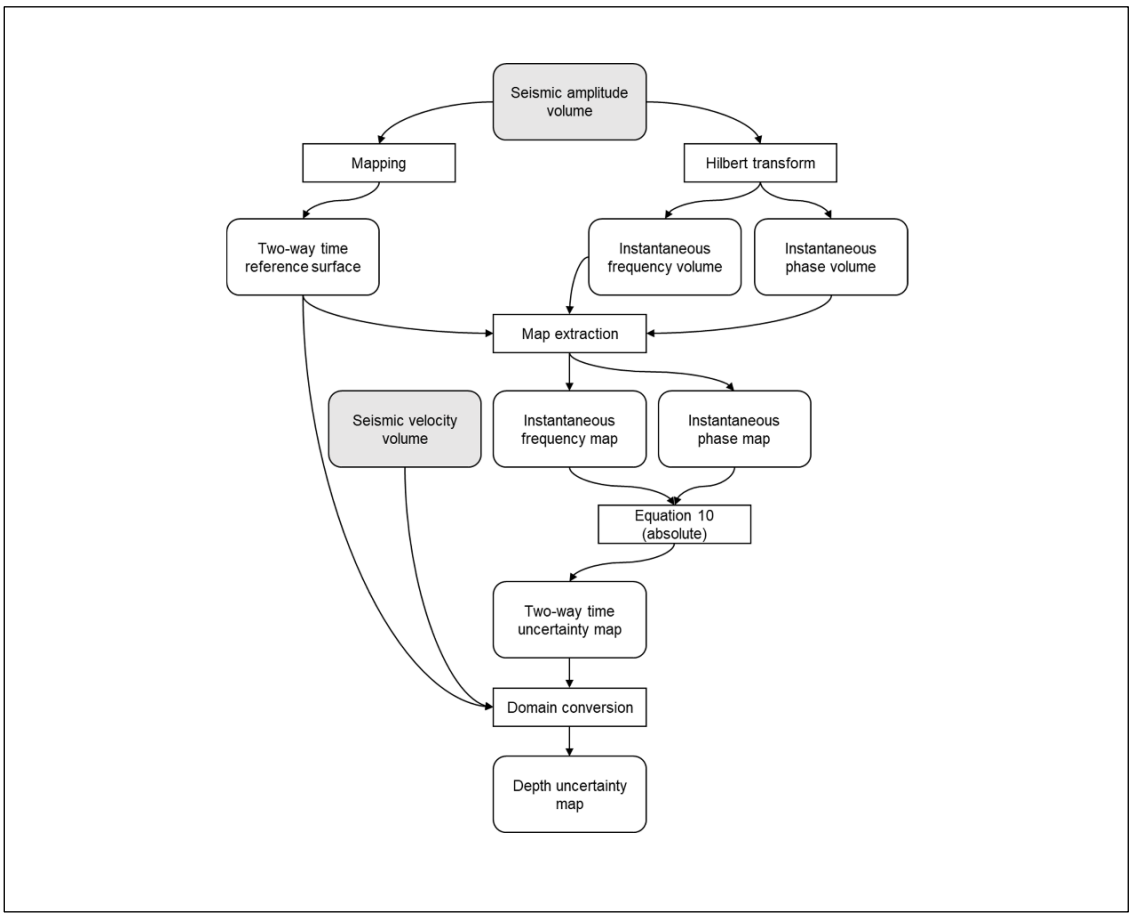

Figure 6: Designed workflow to access the horizon picking uncertainties.

This mineral has higher compressional velocity and density values than the superimposed halite does, characterizing, therefore, an interface with high acoustic impedance contrast (Figure 7). On the other hand, the interface with the lower layer, composed of carbonates from the Pre-Salt section, generally does not represent a relevant impedance contrast, since the average impedances of the carbonate layers are close to the anhydrite impedance, as also illustrated in Figure 7.

To perform the analyses, we built a two-dimensional model, considering the halite, anhydrite, and carbonate lithologies (Figure 8). The acoustic impedance (AI) values considered for each of the three layers are:

(I) Post-Salt section: AI = 12,000 (x 1000 kg·m/s²);

(II) Halite layer: AI = 10,350 (x 1000 kg·m/s²);

(III) Anhydrite layer: AI = 14,850 (x 1000 kg·m/s²);

(IV) Carbonate section: AI = 12,000 (x 1000 kg·m/s²).

The impedance model was transformed into a reflectivity series, which was then convolved with a 15 Hz, zero-phase Ricker wavelet, generating the synthetic seismic section shown in Figure 9.

Next, three more synthetic seismic sections were created, reducing the wavelet phase by 20º each round (Figure 10). The positive peak of the reflector representing the top of the anhydrite layer was picked in the four generated synthetic seismic sections, as can be seen in detail in Figure 11b . It is possible to observe, especially in the synthetic seismic sections of Figure 10, that even phase rotations of 60º do not really change the aspect of the seismic reflector. This means that, considering the simulated conditions, from the interpreter's point of view, the presence of phase (up to 60º) in the data is practically imperceptible.

Then, the time shifts corresponding to the three scenarios with phase shifts were obtained and transformed to depth by a constant speed of 5,500 m/s.

The maximum impact of depth uncertainty over the GRV was estimated for hypothetical scenarios of reservoir isopach assuming 90, 180 and 270 meters, equivalent to 1x, 2x and 3x vertical seismic resolution of a 15 Hz Ricker wavelet (according to the Rayleigh resolution criterion (Kallweit and Wood, 1982), considering a compressional velocity of 5,500 m/s).

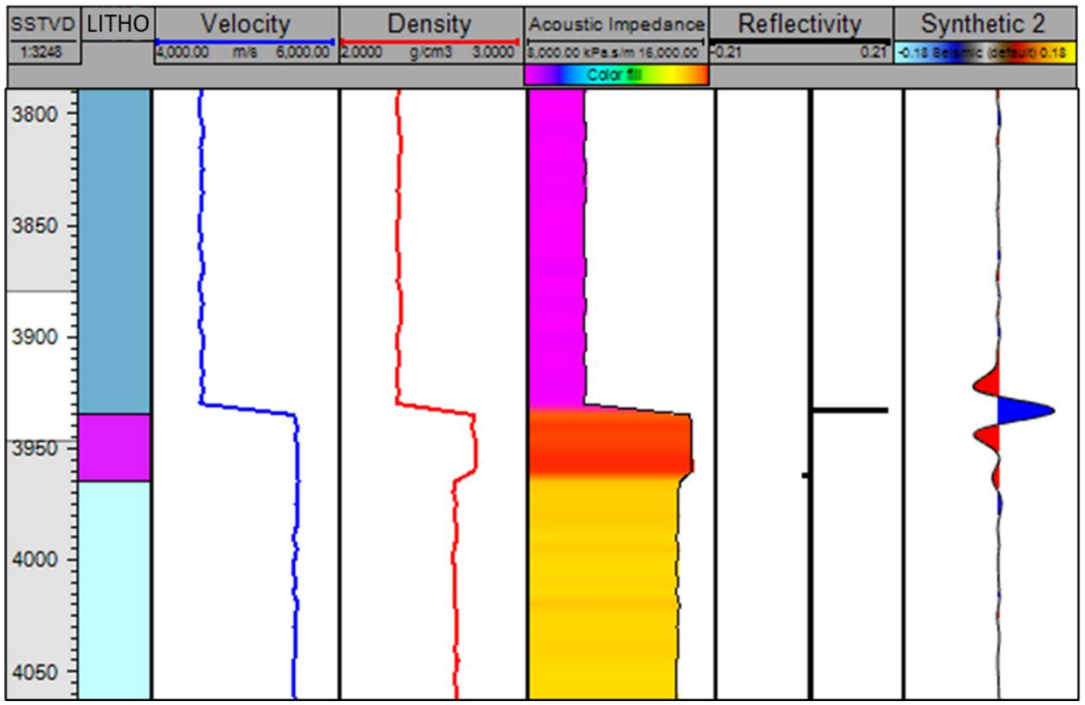

Figure 7: Logs: lithology, compressional velocity, density, acoustic impedance, reflectivity and synthetic seismogram. Built from average values of velocity and density from Campos Basin, Brazil. Ricker wavelet, 15 Hz.

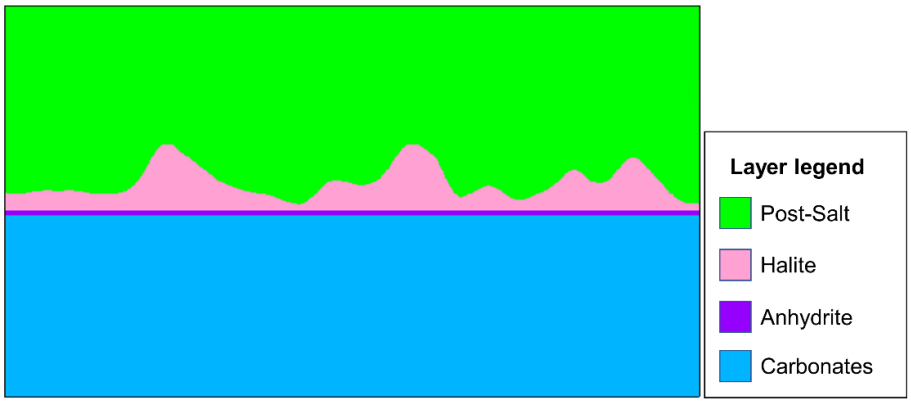

Figure 8: Bidimensional model.

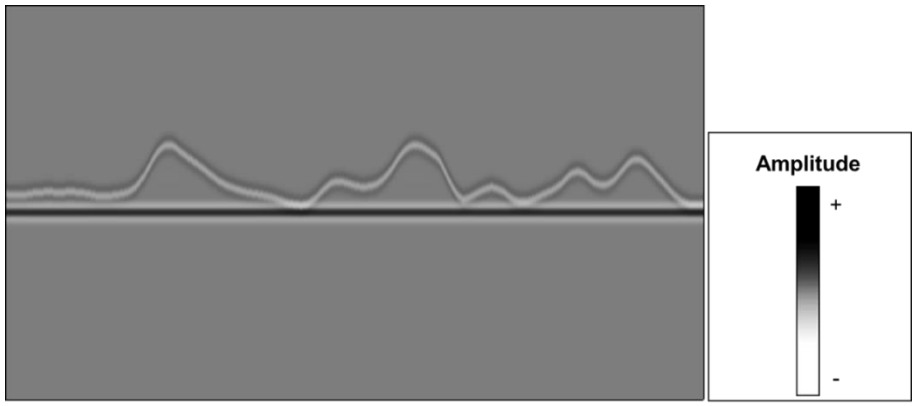

Figure 9: Synthetic seismic section, using zero-phase Ricker wavelet.

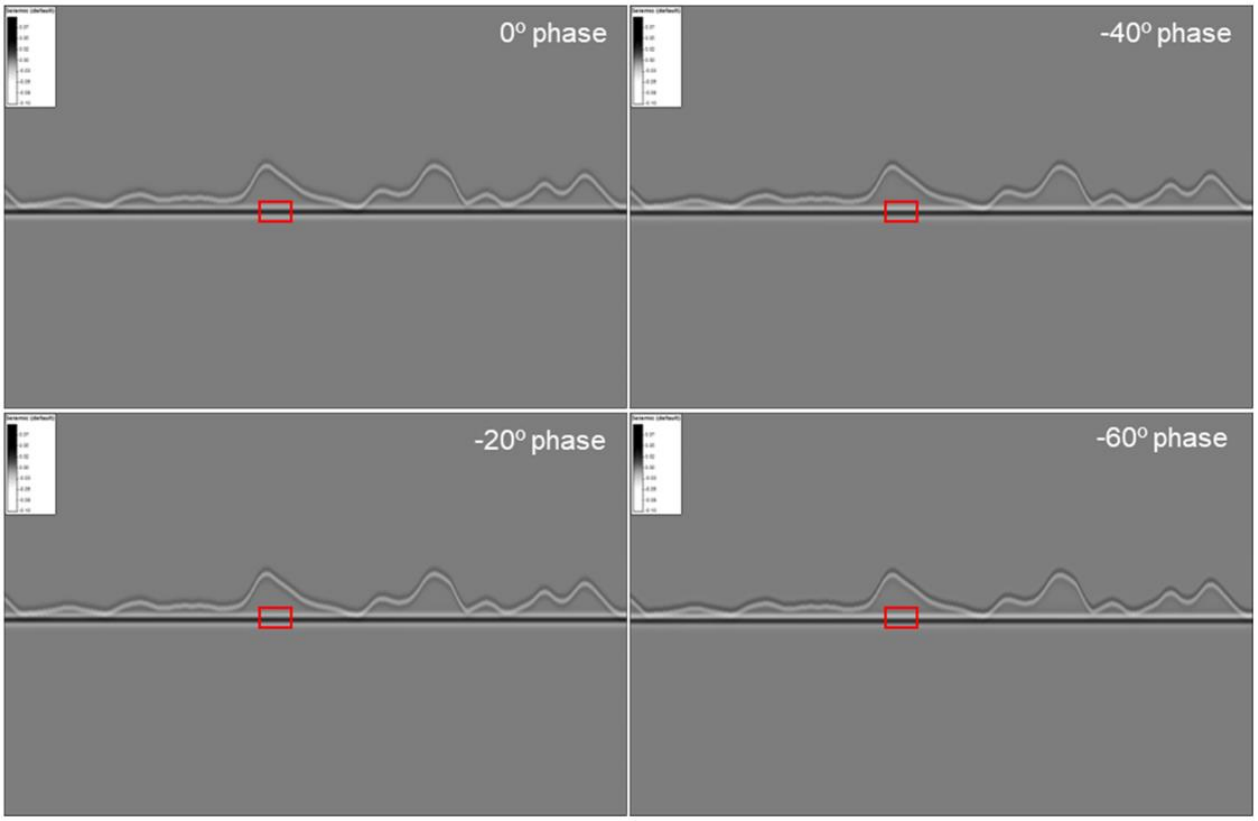

Figure 10: Synthetic seismic sections generated using wavelets with different phases. The red square represents the detailed area shown in Figure 11b.

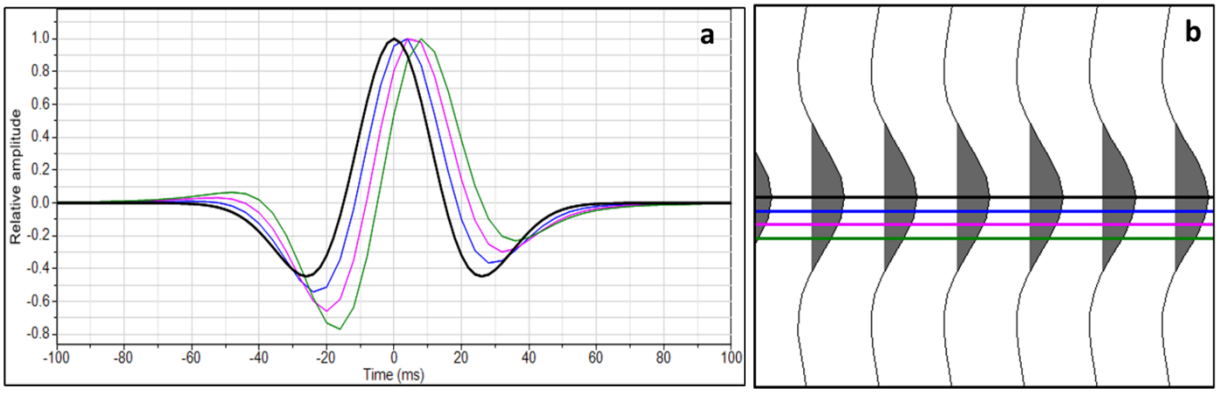

Figure 11: a) Wavelets used to generate synthetic seismic sections; b) Zero-phase seismic section in wiggle format and horizons picked in different phase rotation scenarios.

The results are summarized in the Table 1, where the mapping uncertainty can have different levels of impact on the GRV, depending on the reservoir thickness and the phase present in the data, considering a reference (oil-water contact). It is important to notice that when doing a seismic processing it is not feasible to consider there is a huge problem regarding phase rotation. Therefore, even considering small phase distortions / rotations (e.g., 10°, 20°- maximum – near to real cases) and the depth predictions variation, all the GRV uncertainties arise in the range (3% to 17%) presented by taking different approaches such as salt heterogeneities, signal quality and velocity simulation scenarios (Meyer Viol and Hoetz, 2015; Paes et al., 2019; Maul et al., 2021a, 2021b). We are not advocating for advantages or disadvantages of the previous methods or this suggested one. The main idea is only to deliver one more option to perform GRV uncertainty analysis.

Table 1: Time shift and depth shift values measured in the synthetic model.

Scenario	Time uncertainty (ms)	Depth uncertainty (m)	GRV uncertainty impact (%) 90 m layer	GRV uncertainty impact (%) 180 m layer	GRV uncertainty impact (%) 270 m layer
10° phase	1.39	7.64	8%	4%	3%
20° phase	2.85	15.66	17%	9%	6%
30° phase	4.23	23.27	26%	13%	9%
40° phase	5.59	30.77	34%	17%	11%
50° phase	7.09	38.98	43%	22%	14%
60° phase	8.51	46.80	52%	26%	17%
70° phase	9.87	54.31	60%	30%	20%

Application to real data

The location of the study area is in the northern part of the Campos Basin, 60 km off the east coast of Brazil (Figure 12). Its stratigraphy includes Late Cretaceous to early sediments (Figure 13). The methodology was applied to the seismic horizon that represents the top of the carbonate reservoir of Aptian age in the area.

We used 3D high-resolution time-domain seismic survey data to map the reference surface corresponding to the base of the evaporitic section (Figure 14 and Figure 15) and to generate the seismic attributes of the complex trace (Figure 15b, 15c and 15d).

By applying the proposed methodology (Figure 6), the time uncertainty map was calculated using equation 10 and converted from the time to depth domain by multiplying by the compressional velocity map, generating the depth uncertainty map (Figure 16).

Uncertainty quantification – GRV simulations

To estimate the impact of the horizon picking uncertainty by the proposed methodology, we used a stochastic approach as described by Meyer Viol and Hoetz (2015), where multiple realizations of the top surface are made and a GRV expectation curve is generated, considering the oil-water contact, of known depth, as lower limit. Each realization is constructed from the mapped surface using Sequential Gaussian Simulation (SGS) (Figure 17).

The base case considered (Z_{BC}) is the surface corresponding to the top of the carbonate reservoir, originally mapped in time and converted to depth by the velocity model. Each realization is defined as (Meyer Viol and Hoetz, 2015):

$$Z_{rel,n} = Z_{BC} + Z_{err,n} \quad (11)$$

where

$$Z_{err,n} = \Delta Z \cdot Z_{ran,n}$$

where ΔZ is the depth uncertainty map and $Z_{ran,n}$ is a map generated by the SGS algorithm to randomly assign a value between -1 and 1 to each location of the study area. The variogram used has an alignment of 45^0 and dimensions of 4 km x 2 km to better represent the preferred structural direction, which can be observed in the map at Figure 17.

Once each realization of the reservoir top is created, the GRV can be calculated considering the oil-water contact. After this process was done for each realization (100 realizations were made) (Figure 18), the GRV was calculated from all realizations and plotted on an expectation curve (Figure 19).

For the deterministic case ($\boldsymbol{Z_{BC}}$), the estimated GRV between the top of the reservoir and the considered oil-water contact is 72.5 MM m³. Hundred possible structural tops were generated by SGS considering a variogram whose the largest dimension is aligned at 45º, with dimensions 4 km x 2 km. The GRV from all realizations was calculated and plotted on an expectation curve (Figure 19). The volume P10 and P90 are, respectively, 69 MM m³ and 78 MM m³, or 0.95 and 1.07 times the deterministic case volume. This represents a variation of near 5%, up or down from the base case volume. Once again, this range of variation is totally in accordance with previous studies done in the Campos and Santos basins, considering GRV variations (Paes et al., 2019; Maul et al., 2021a, 2021b). The synthetic case was performed to understand the mathematical limits of the methodology. However, we only consider mathematical cases near to real cases, i.e., up to 20°- maximum of phase distortions/rotations.

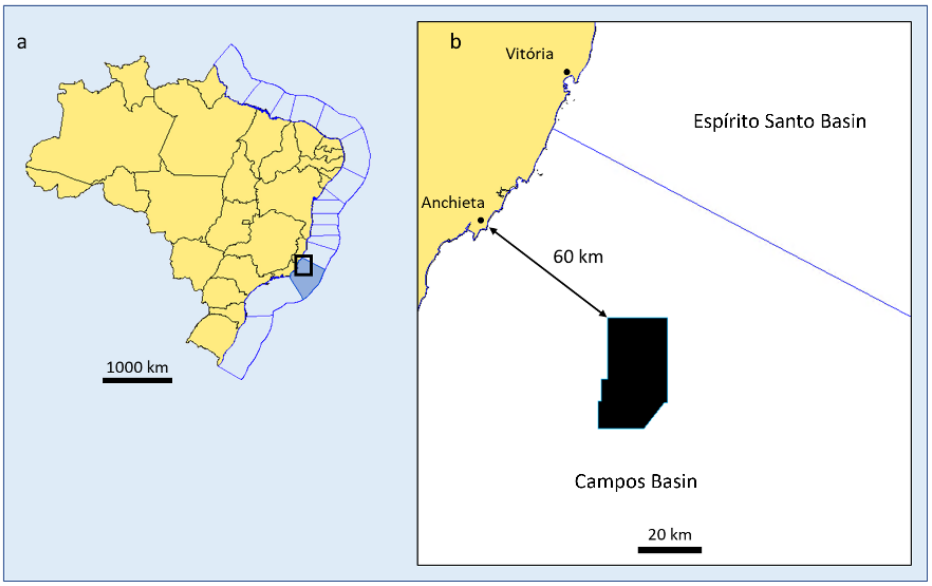

Figure 12: a) location map of the Campos Basin; b) location of the study area (3D seismic survey) highlighted by the black filled polygon.

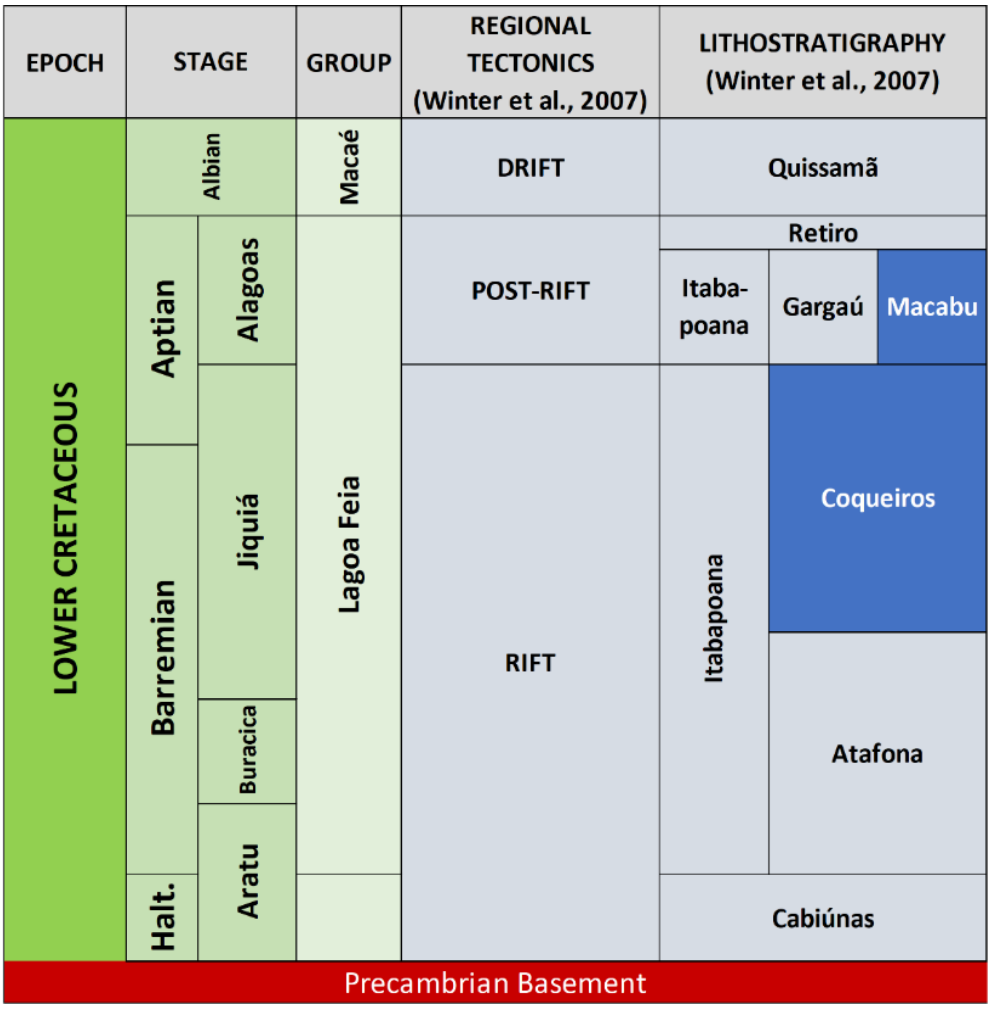

Figure 13: Stratigraphic and tectonic framework of the Campos Basin in the study area. Lithostratigraphy, ages and tectonics are based on Winter et al. (2007).

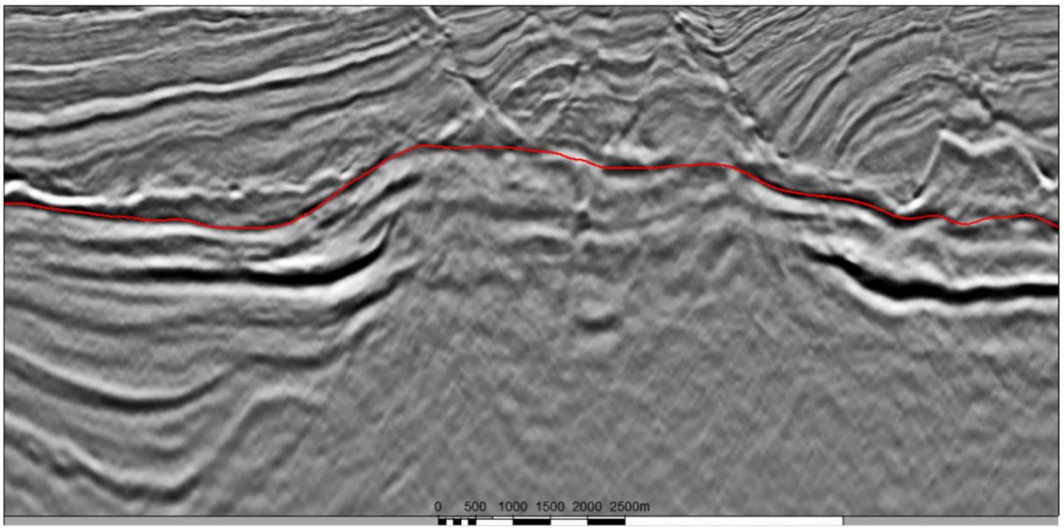

Figure 14: NW-SE seismic section and mapped reference surface (in red). Figure 15a shows the position of this section.

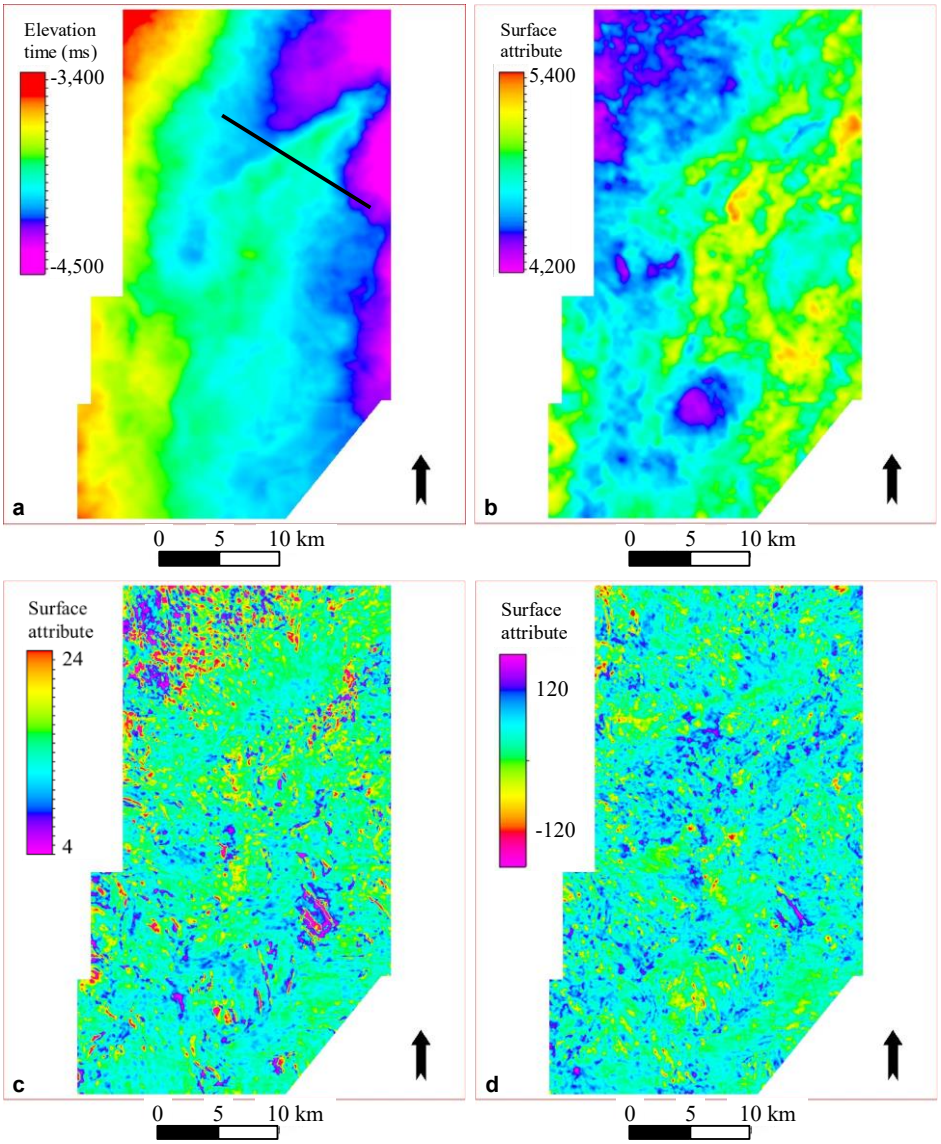

Figure 15: a) Reference surface in two-way time; b) compressional velocity; c) instantaneous phase; d) instantaneous frequency.

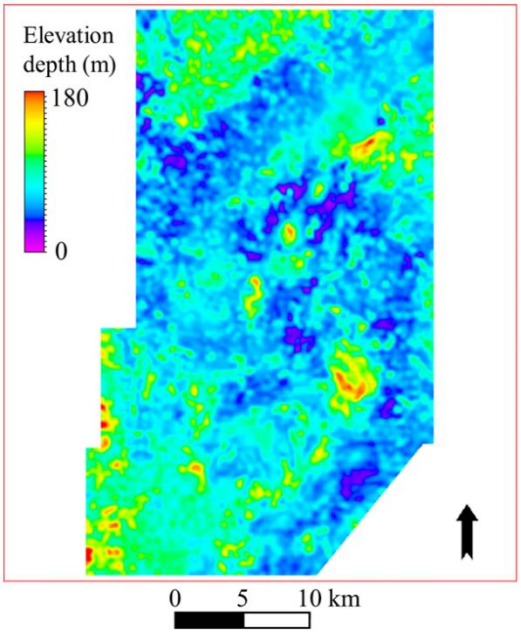

Figure 16: Depth uncertainty map calculated from the proposed methodology.

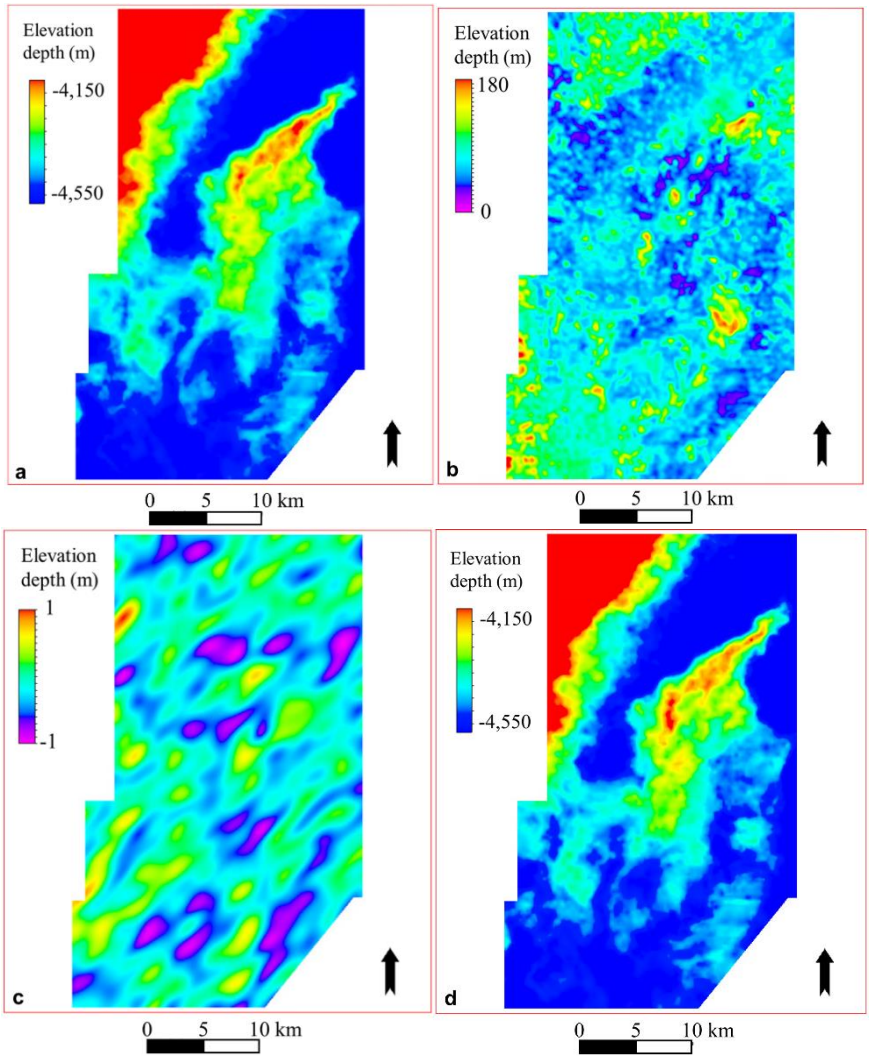

Figure 17: a) depth reference surface map; b) depth uncertainty map; c) random map generated by the SGS algorithm; d) one surface Z_{rel} realization.

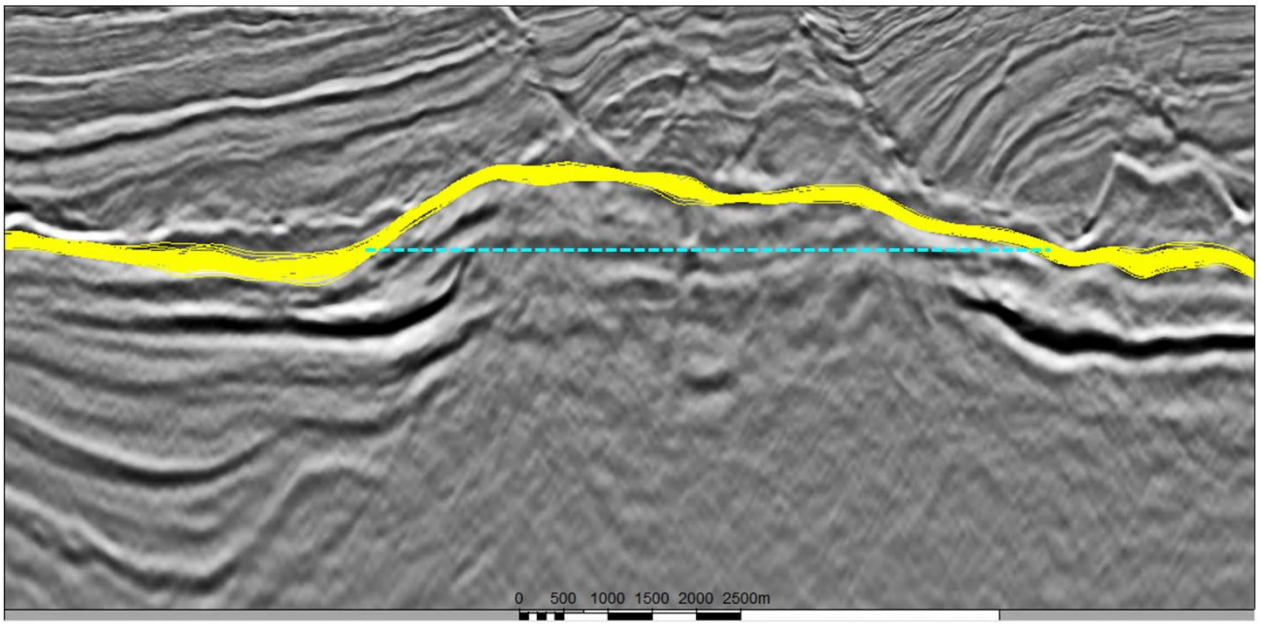

Figure 18: Seismic section with 100 surface realizations (yellow). The dashed blue line represents the considered oil-water contact.

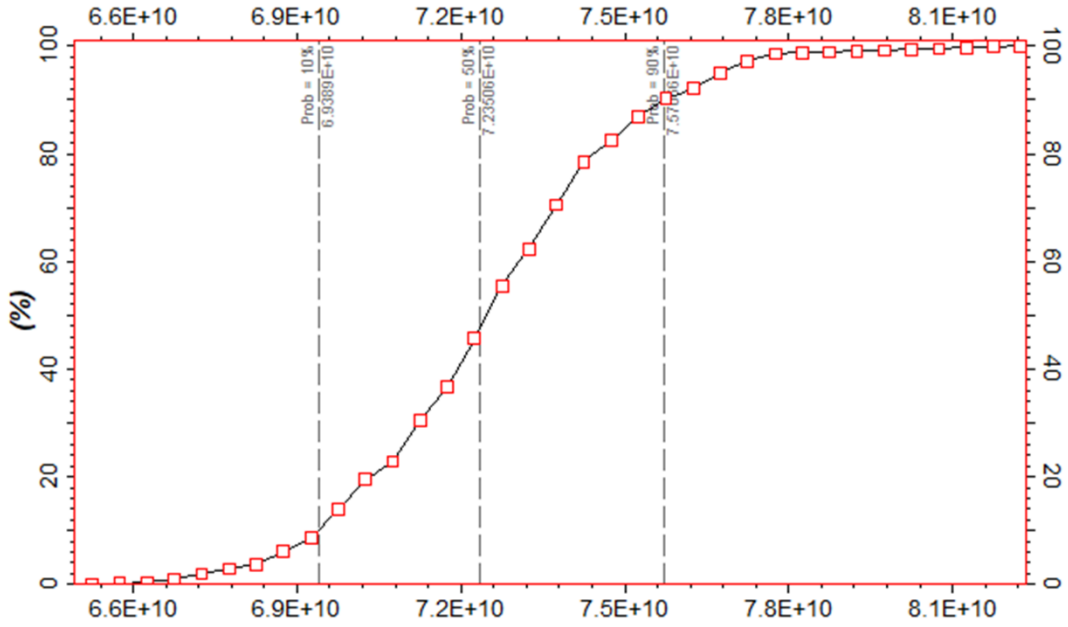

Figure 19: GRV expectation curve from 100 realizations.

CONCLUSION

The seismic mapping uncertainties were translated into uncertainty about a parameter of economic interest: gross rock volume (GRV). Applying the methodology to synthetic seismic data, we measured the potential relevance of this uncertainty in relation to the variation of the GRV for different scenarios, and it was possible to conclude that the impact of this uncertainty is dependent on the thickness of the layer considered. Applied to real data, the methodology showed that the mapping uncertainty introduced uncertainties of the order of 5% in the gross volume of rock, totally in accordance with the ranges observed in other studies, following distinct methodologies.

These results highlight the importance of taking mapping uncertainty into account when estimating reserves and other economic parameters, and the proposed methodology is an objective way of evaluating and quantifying this type of uncertainty in real data.

Data and Materials Availability

The seismic dataset used and/or analyzed during the current study are not publicly available due to Brazilian National Agency of Petroleum, Natural Gas and Biofuels (ANP) restrictions.

ACKNOWLEDGMENTS

The authors would like to express their gratitude to Petróleo Brasileiro S.A. (Petrobras) for granting permission to conduct this study during a MSc project at Universidade Federal Fluminense (UFF) and for providing data and tools for the research. We also thank the Brazilian National Agency of Petroleum, Natural Gas and Biofuels (ANP) for permission to use the data in this study. Additionally, we extend our appreciation to the Exploratory Interpretation and Reservoir Characterization Group (GIECAR) at UFF for academic support. Finally, we would like to express our gratitude to the reviewers for dedicating their time and providing detailed suggestions, which greatly contributed to the preparation of the final version.

REFERENCES

Barton, N., 2007, Rock Quality, Seismic Velocity, Attenuation and Anisotropy. Taylor & Francis Group, London, UK: CRC Press. 729 pp. https://doi.org/10.1201/9780203964453.

Boashash, B. ed., 2016, Chapter 1 - Time-Frequency and Instantaneous Frequency Concepts, *in* B. Boashash, ed., Time-Frequency Signal Analysis and Processing: 2nd ed., 31–63. Oxford: Academic Press. https://doi.org/10.1016/B978-0-12-398499-9.00001-7.

Bouchaala, F., M.Y. Ali, J. Matsushima, Y. Bouzidi, E.M.T. Takougang, A.A.I. Mohamed and A.A. Sultan, 2019, Scattering and Intrinsic Attenuation as a Potential Tool for Studying of a Fractured Reservoir: Journal of Petroleum Science and Engineering, **174**, 533–543. https://doi.org/10.1016/j.petrol.2018.11.058.

Camargo, G.N., M. González, F. Borges, A. Maul, and W.U. Mohriak, 2023, Challenges for Seismic Velocity Modelling of Rafts and Impacts for Pre-Salt Depth Estimations: Petroleum Geoscience, **29**, no. 1, petgeo2022-033. https://doi.org/10.1144/petgeo2022-033.

Charles, T., J.M. Guemene, B. Corre, G. Vincent, and O. Dubrule, 2001, Experience with the Quantification of Subsurface Uncertainties: SPE Asia Pacific Oil and Gas Conference and Exhibition. Jakarta, Indonesia, Society of Petroleum Engineers. https://doi.org/10.2523/68703-MS.

Hardage, B., 2010, Instantaneous Seismic Attributes Calculated by the Hilbert Transform. Search and Discovery, no. 40563.

Kallweit, R.S. and L.C. Wood, 1982, The Limits of Resolution of Zero-phase Wavelets: GEOPHYSICS, **47**, no. 7, 1035–46. https://doi.org/10.1190/1.1441367.

Kjartansson, E., 1979, Constant Q-wave propagation and attenuation: Journal of Geophysical Research, **84**, 4737–4748. https://doi.org/10.1029/JB084iB09p04737.

Kolsky, H., 1956, LXXI. The propagation of stress pulses in viscoelastic solids. The Philosophical Magazine: A Journal of Theoretical Experimental and Applied Physics, **1**, no. 8, 693–710. https://doi.org/10.1080/14786435608238144.

Leahy, G.M. and A. Skorstad, 2013, Uncertainty in Subsurface Interpretation: A New Workflow: First Break, **31**, no. 9, 87–93. https://doi.org/10.3997/1365-2397.31.9.71079.

Levy, S. and D.W. Oldenburg, 1987, Automatic Phase Correction of Common-midpoint Stacked Data: GEOPHYSICS, **52**, no. 1, 51–59. https://doi.org/10.1190/1.1442240.

Liner, C.L., 2012, Elements of Seismic Dispersion: A Somewhat Practical Guide to Frequency-Dependent Phenomena: Society of Exploration Geophysicists, **15**, 193 pp. https://doi.org/10.1190/1.9781560802952.

MacDonald, A., K. Zhang, J.I. Tollefsrud, and R. Chelak, 2009, Introduction to Reservoir Uncertainty Modeling: GeoConvention 2009, 802–5.

Matos, M.C. De, K.J. Marfurt, and P.R.S. Johann, 2010, Seismic Interpretation of Self-Organizing Maps Using 2D Color Displays: Revista Brasileira de Geofisica, **28**, no. 4, 631–42. https://doi.org/10.1590/S0102-261X2010000400008.

Maul, A., M. Cetale, C. Guizan, P. Corbett, J.R. Underhill, L. Teixeira, R. Pontes, L. Falcão, T. Yamamoto, and M. González, 2021a, Insertion of Salt Stratification When Building Detailed Velocity Models and Its Impacts Regarding Uncertainties Analysis for Gross-Rock Volumes Estimation: 17th International Congress of the Brazilian Geophysical Society. Rio de Janeiro, Brazil, https://doi.org/10.22564/17cisbgf2021.185.

Maul, A., M. Cetale, C. Guizan, P. Corbett, J.R. Underhill, L. Teixeira, R. Pontes, L. Falcão, T. Yamamoto, and M. González, 2021b, The Impact of Heterogeneous Salt Velocity Models on the Gross Rock Volume Estimation: An Example from the Santos Basin Pre-Salt, Brazil: Petroleum Geoscience, **27**, no. 4, petgeo2020-105. https://doi.org/10.1144/petgeo2020-105.

Meyer Viol, S. L. and H.L.J. Hoetz, 2015, Uncertainty in Gross Rock Volume Analysis - A Stochastic or Deterministic Approach?: 77th EAGE Conference and Exhibition 2015: Earth Science for Energy and Environment, Madrid, Spain, 2592–2596. https://doi.org/10.3997/2214-4609.201413034.

Müller, T. M., B. Gurevich, and M. Lebedev, 2010, Seismic Wave Attenuation and Dispersion Resulting from Wave-Induced Flow in Porous Rocks — A Review: GEOPHYSICS, **75**, no. 5, 75A147–64. https://doi.org/10.1190/1.3463417.

Nunes, B. I. C., W.E. De Medeiros, A.F. Nascimento, Do. and J.A.M. Moreira, 2011, Estimating Quality Factor from Surface Seismic Data: A Comparison of Current Approaches: Journal of Applied Geophysics, **75**, no. 2, 161–170. https://doi.org/10.1016/j.jappgeo.2011.07.003.

Paes, M., C.M.C. Pereira, V. Pinto, A.R.M. Maul, T. Meneguim, G. Gonzalez, R.S. Meyer, and S.L. Furland, 2019, Brazilian Pre-Salt Gross-Rock Volume Uncertainties: Integration between Velocity Model and Seismic Resolution: 81st EAGE Conference and Exhibition 2019, 1–5. London, UK: European Association of Geoscientists and Engineers, https://doi.org/10.3997/2214-4609.201901460.

Pinto, V.R., C.E.B.S. Abreu, R.C. Monteiro, J. Rosseto, and G.M. Leahey, 2017, Seismic Uncertainty Estimation in Reservoir Structural Modelling: First Break, **35**, no. 10, 51–54. https://doi.org/10.3997/1365-2397.35.10.90243.

Roden, R. and H. Sepúlveda, 1999, Significance of Phase to the Interpreter: Practical Guidelines for Phase Analysis: The Leading Edge, **18**, no. 7, 774–777. https://doi.org/10.1190/1.1438375.

Rosa, A.L.R., 2018, Análise do Sinal Sísmico. 2nd ed. Rio de Janeiro, Brazil: Sociedade Brasileira de Geofísica, 713 pp.

Samson, P., O. Dubrule, and N. Euler, 1996, Quantifying the Impact of Structural Uncertainties on Gross-Rock Volume Estimates: NPF/SPE European 3-D Reservoir Modelling Conference, 381–392. https://doi.org/10.2523/35535-ms.

Simm, R. and M. Bacon, 2014, Seismic Amplitude: An Interpreter's Handbook. Cambridge: Cambridge University Press. 271 pp. https://doi.org/10.1017/cbo9780511984501.

Simm, R. and R. White, 2002, Phase, Polarity and the Interpreter's Wavelet: First Break, **20**, 277–281. https://doi.org/10.1046/j.1365-2397.2002.00277.x.

Souza, W.E., R. R. Manenti, and M.J. Porsani, 2017, Automatic First-Breaks Picking Using Linear Moveout Correction and Complex Seismic Traces: Revista Brasileira de Geofísica, **34**, no. 3, 319–326. https://doi.org/10.22564/rbgf.v34i3.823.

van der Baan, M., 2008, Time-Varying Wavelet Estimation and Deconvolution by Kurtosis Maximization: GEOPHYSICS, **73**, no. 2, 11–18. https://doi.org/10.1190/1.2831936.

Wang, Y., 2008, Seismic Inverse *Q* Filtering: Blackwell Publishing, 248 pp.

Winter, W.R., R.J. Jahnert, and A.B. França, 2007, Bacia de Campos: Boletim de Geociências da Petrobras, **15**: 511–529.

Wu, J., Q. Liu, X. Zhang, C. Zhou, X. Yin, W. Xie, X. Liang, and J. Huang, 2022, Attenuation Characteristics of Impact-Induced Seismic Wave in Deep Tunnels: An in Situ Investigation Based on Pendulum Impact Test: Journal of Rock Mechanics and Geotechnical Engineering, **14**, no. 2, 494–504. https://doi.org/10.1016/j.jrmge.2021.12.005.

Yilmaz, O., 2001, Seismic Data Analysis: 2nd ed., 2 vols., Society of Exploration Geophysicists. https://doi.org/10.1190/1.9781560801580.

Jardim, F.: conceptualization, formal analysis, investigation, methodology, project administration, software, validation, writing – original draft; **Maul, A.R.:** conceptualization, investigation support, methodology support, supervision support, validation, writing – original draft support; **Lupinacci, W. M.:** conceptualization support, investigation support, methodology support, supervision support, validation support, writing – original draft support.

Received on December 27, 2023 / Accepted on May 06, 2024